RSC Advances

ROYAL SOCIETY OF CHEMISTRY

www.rsc.org/advances

Effects of electrolyte concentration and synthesis methods of sulfur/carbon composites on the electrochemical performance in lithium-sulfur batteries

Guochun Li, Wen Zhao, Liang Liu*, Long Chen

Automotive Engineering Research Institute, Jiangsu University, Zhenjiang 212013, China

*Corresponding author. Tel./Fax: +86 511 88782845. E-mail address: lliu@mail.ujs.edu.cn

Abstract

Three synthesis methods are adopted in this study for the preparation of sulfur/carbon composites for rechargeable lithium-sulfur batteries, namely, melting (155 °C)-vaporizing (300 °C), ball milling, and ball milling-melting (155 °C). The structure, composition, and morphology of the samples are characterized by Brunauer-Emmett-Teller (BET), thermogravimetric (TG) analysis, X-ray diffraction (XRD), scanning electron microscopy (SEM), and elemental mapping analysis. The effects of electrolyte concentration and synthesis methods on the electrochemical performance of composites are also investigated. Results show that active sulfur disperses with carbon matrix more uniformly in the sulfur/carbon composite prepared by melting-vaporizing method. The assembled cell delivers an extraordinarily high initial discharge capacity of 1856.2 mAh g^{-1} when measured in the electrolyte with 5 M LiTFSI in DOL/TEGDME at a current density of 160 mA g^{-1}; the capacity can still be retained at 905.3 mAh g^{-1} after 125 cycles. When measured at a higher current density of 800 mA g^{-1}, a reversible capacity of 546.3 mAh g^{-1} can be maintained after 500 long-term cycles. The preferable electrochemical performance of the composite electrode is attributed to the high dispersibility of the carbon matrix and active sulfur in the composite, as well as the high concentration of lithium salt in the

electrolyte. This work provides an optimized approach to obtain sulfur/carbon composites with remarkably improved electrochemical performance for lithium-sulfur batteries.

Keywords: lithium-sulfur batteries; electrolyte concentration; synthesis methods; carbon black; electrochemical performance

1. Introduction

Elemental sulfur as cathode material offers an attractive specific capacity of 1672 mAh g^{-1}, which is nearly one order of magnitude higher than those of state-of-the-art Li-ion battery insertion cathodes. Moreover, sulfur is inexpensive, naturally abundant, and non-toxic. Therefore, rechargeable lithium-sulfur batteries are regarded as one of the most promising candidates for next-generation energy storage devices.[1-6] Although lithium-sulfur batteries have been investigated for several years, issues of low utilization of active material, rapid capacity degradation, and poor rate capability have not been completely settled, thereby seriously hindering the practical applications of Li-S batteries in the commercial market.[7,8] To address the aforementioned problems, considerable attempts have been made regarding whole battery components; for example, configuration of sulfur-based composites,[9-25] optimization of electrolytes[26-30] and binders,[31-34] as well as modification of lithium anode[35,36] and separators.[37-39] Among them, one of the most commonly used strategies is to construct sulfur-based composites, especially sulfur-carbon composites, and reversible capacity ranging between 1000 to 1400 mAh g^{-1} (calculated by sulfur) can be easily achieved. Up to present, numerous studies have focused on the design and construction of carbon materials themselves. However, little attention has been paid to

the synthetic procedures of sulfur/carbon composites. As a complex electrochemical system for energy storage and conversion, there are many factors that directly impact the performance of a Li-S battery, such as carbon/sulfur ratio, sulfur loading density, electrolyte volume and electrode deformability.[40] In addition, the microstructures of the as-prepared samples are known to exert considerable effects on the electrochemical behavior, as well. Therefore, to tune the microstructure parameters so as to improve the electrochemical performance of lithium-sulfur batteries, the optimization of preparation conditions needs consideration. To date, various synthetic routes have been developed to obtain sulfur/carbon composites.[5] To summarize, the following two routes are primarily available: (1) solid-phase synthesis routes, which include ball milling and heat treatment; and (2) liquid-phase synthesis routes, which include chemical reaction deposition and physical dissolution-reprecipitation of sulfur. In the present paper, we use a commercial carbon black to study the effect of the synthesis methods of sulfur/carbon composites on electrochemical performance in lithium-sulfur batteries. Meanwhile, solid-phase synthetic routes are introduced because of their feasible, low-cost, and eco-friendly preparation processes. We report sulfur/carbon composites that are synthesized by three different routes: melting (155 °C)-vaporizing (300 °C), ball milling, and ball milling-melting (155 °C). Furthermore, recent reports have shown that ether-based electrolytes with different concentrations of lithium salt are crucial for the utilization of active sulfur and cycle stability of sulfur cathodes,[21,29] because the dissolution of lithium polysulfides can be suppressed based on the “common ion effect” and high viscosity in electrolyte with concentrated lithium salt. Therefore, we demonstrate the significance of electrolyte concentration and synthesis methods of sulfur/carbon composites and show how these factors influence the electrochemical results in lithium-sulfur batteries.

2. Experimental

S/KB composites preparation

Commercial carbon black (Ketjenblack EC600JD, Cabot Corporation) was purchased from Shanghai Fuhua Industrial Company. Before use, the carbon black was ball-milled to powder in a planetary type ball mill (QM-3SP2, 300 rpm, 12 h), which was denoted as KB. Sulfur powder (sublimed, 100 mesh, 99.5%) was purchased from Alfa Aesar and used without further treatment. Both ball milling and heat treatment methods were performed under Ar atmosphere to prevent conceivable oxidation of sulfur.

Sulfur/carbon composites were prepared through three different synthesis methods. For melting (155 °C)-vaporizing (300 °C) method, carbon black was mixed with sulfur power at a weight ratio of 1:4. The mixture was then placed in a sealed stainless steel vessel, heated to 155 °C with a heating rate of 5 °C min^{-1}, and maintained at the temperature for 5 h. Then, the temperature was increased to 300 °C and held for another 2 h to vaporize the residual sulfur covering the surface of the carbon matrix. After cooling down to room temperature, a composite with 60 wt.% S was obtained and marked as S/KB-1. For comparison, another two samples with the same sulfur content were marked as S/KB-2 and S/KB-3, respectively. For ball-milling method (S/KB-2), carbon black and sulfur powder (mass ratio: 4/6) were ball-milled for 5 h at a speed of 300 rpm. Finally, for ball-milling-melting (155 °C) method (S/KB-3), the carbon black and sulfur powder (mass ratio: 4/6) were first ball-milled for 5 h at a 300 rpm speed, and then heated to 155 °C and maintained at the temperature for 12 h.

Materials characterization

The microstructure and morphology of carbon black and as-prepared S/KB composites were detected by Brunauer-Emmett-Teller (BET, JW-BK instrument, Beijing), X-ray diffraction (XRD, Rigaku MiniFlex II)), and scanning electron microscopy (SEM, HITACHI S-4800). Elemental mappings of carbon and sulfur were carried out by local chemical analysis, which is performed by STEM-EDX with a HAADF detector. Sulfur content in composites were confirmed by thermal gravimetric analysis (TGA, Mettler-Toledo) from 30 °C to 600 °C, with a heating rate of 10 °C min^{-1} under Ar.

Electrochemical measurements

To prepare sulfur cathodes, S/KB composite pastes were firstly prepared by mixing the S/KB composite (70 wt.%), acetylene black (20 wt.%), and PTFE (10 wt.%) with ethanol as dispersant. The paste was then compressed onto thin pieces with a roller. The composite electrode were punched into a disc of 8 mm diameter and dried at 55 °C for 12 h. The mass for each disc was 1.2~1.5 mg，while the active materials area loading for each electrode was 1.0~1.25 mg cm^{-1}. Half-cells were assembled in an Ar-filled glove box. Lithium metal was used as counter electrode and reference electrode, and microporous Celgard-2300 was used as a separator. The electrolytes were ether-based and composed of 1 M to 5 M bis(trifluoromethanesulfonyl)imide (LiTFSI) combined with 0.2 M $LiNO_3$ dissolved in mixed solvents of 1,3-dioxolane (DOL)/tetraethylene glycol dimethyl ether (TEGDME) with a volume ratio of 1:1. The cells were galvanostatically charged-discharged in the potential range of 1.0 V to 3.0 V (versus Li/Li^+) on the basis of mass sulfur at various current densities at ambient temperature using a LAND-CT2001A instrument (Wuhan Jinnuo, China). Electrochemical impedance spectroscopy (EIS) of half-cells were measured at a discharge state by using Zahner Zennium electrochemical workstation at a

frequency range of 100 kHz to 10 mHz, whereas the disturbance amplitude was set to be 5 mV.

3. Results and discussion

The image in Fig. 1 shows the sulfur content in the S/KB composites, which were detected by TGA, performed from 30 °C to 600 °C under Ar atmosphere. Evidently, the sulfur content for all three composites that are calculated from TG curves are approximately 60 wt.%. The weight loss for S/KB-1 occurs at about 150 °C and terminates at about 380 °C, while for S/KB-2 and S/KB-3, weight loss occurs at about 180 °C and terminates at about 430 °C. Notably, the TG curves of S/KB-2 and S/KB-3 are similar, for which occurring and terminating temperature are later than those of S/KB-1.

The specific surface areas and pore volumes of KB and the as-prepared S/KB composites prepared by different synthesis methods are shown in Tab. 1. In addition, the nitrogen adsorption-desorption isotherms, combined with the pore size distribution curves of KB and S/KB composites are presented in Fig. S1-S2, as well. Prior to nitrogen adsorption-desorption measurements, all samples were degassed at 60 °C for 0.5 h. As seen, the meso-porous carbon KB exhibits a high specific surface area of 1007.21 $m^2 g^{-1}$ and a large pore volume of 2.03 $cm^3 g^{-1}$. After loading sulfur, however, specific surface areas are sharply reduced to 129.84, 205.69, and 221.39 $m^2 g^{-1}$, and the corresponding pore volumes are also simultaneously decreased to 0.259, 0.315, and 0.348 $cm^3 g^{-1}$ for S/KB-1, S/KB-2 and S/KB-3 composites, which are prepared by melting (155 °C)-vaporizing (300 °C), ball-milling, and ball-milling-melting (155 °C), respectively. Such a dramatic decrease in specific surface areas and pore volumes implies that active sulfur is successfully impregnated into nanopores or loaded onto the surface of the carbon

matrix.[18]

The SEM images of KB and the as-prepared S/KB composites are presented in Fig. 2. The image in Fig. 2a shows that KB appears as a loose particle aggregation of several small carbon nanospheres with an average diameter of 50 nm. For S/KB-1 composite, morphology remained virtually unchanged in comparison with KB. Moreover, though the size of S/KB-1 particles slightly increased, no large bulk sulfur particles are detected on the surface of the carbon matrix. This finding indicates that sulfur with lowest viscosity was diffused and embedded into the pores of the carbon matrix during heat treatment at 155 °C, and then further vaporizing of extra sulfur on the surface of KB at 300 °C. For the S/KB-2 composite, the aggregates became denser and rougher, which was induced in the ball-milling process of carbon black and sulfur. In addition, after heat treatment of the S/KB-2 composite at 155 °C, the particles became larger and certain large bulks were formed, as presented in Fig. 2d.

The presence and distribution of sulfur and carbon are further confirmed by local chemical analysis, performed by STEM-EDX (Fig. 3). Evidently, the elements of sulfur and carbon can be detected through the entire area of the three S/KB samples, confirming the existence of sulfur and carbon in the composites. In particular, elemental sulfur and carbon show homogeneous distribution in the S/KB-1 composite, suggesting a highly dispersed state of sulfur and carbon in the composite, as presented in Fig. 3a and in consistent with SEM and XRD observations (Fig. S3). On the other hand, partial enrichment of sulfur or the lack of carbon in S/KB-2 and S/KB-3 composites present heterogeneous distribution, which is due to partial aggregation in S/KB-2 and S/KB-3 composites.

To investigate the effect of electrolyte concentration on the cycle performance of Li-S

batteries, the S/KB-1 composite was selected for investigation and measurement in ether-based electrolytes that contain different concentrations of lithium salt (LiTFSI) and 0.2 M $LiNO_3$ additive dissolving in the mixed solvents of 1,3-dioxolane (DOL)/tetraethylene glycol dimethyl ether (TEGDME) at a current density of 160 mA g^{-1}. As seen in Fig. 4a, cells with higher concentration of lithium salt exhibit superior cycle stability. For cells measured in electrolytes with 1, 2, and 3 M LiTFSI, initial discharge capacities of 1859.6, 1602.6 and 1238 mAh g^{-1} can be obtained. However, the capacities sharply decreased to 325.3, 540.6, and 658.8 mAh g^{-1} after 50 cycles. Meanwhile, for the cell measured in the electrolyte with 5 M LiTFSI, an initial discharge capacity of 1856.2 mAh g^{-1} is obtained, and the reversible capacity can still be retained at 888.6 mAh g^{-1} after 50 cycles, showing better capacity retention capability and utilization of active sulfur. Results indicate that a high concentration of lithium salt favors electrochemical performance by effectively suppressing polysulfide dissolution into electrolytes, which is due to "common-ion effect".[29] The corresponding initial, 10^{th}, and 50^{th} charge-discharge curves of the S/KB-1 composite measured in four electrolytes with different lithium salt concentrations are shown in Figs. 4b to 4e, respectively. Evidently, two typical discharge plateaus at about 2.30 and 2.05 V (versus Li/Li^+) could be seen from the discharge curves of the four samples, corresponding to two-step reactions of elemental sulfur with metallic lithium.[9,14] In addition, a low and long potential plateau at around 1.20 V could be observed in the initial discharge process, which may be attributed to the existence of weak interaction between carbon and sulfur in the composite. The phenomenon for such an excess capacity can be found elsewhere.[16] Moreover, other study reported that when the battery was discharged below 1.5 V, $LiNO_3$ as co-salt will be reduced, which appears as "capacity". This could be another reason for the obtained capacity higher than

the theoretical value of 1672 mAh g^{-1}.[41] However, the plateau disappeared in the succeeding cycles, resulting in a dramatic capacity decay as compared with the first cycle. During the charge process, only one potential plateau at around 2.31 V is presented, corresponding to interlaced conversions from lithium sulfides to low-order lithium polysulfides, high-order lithium polysulfides, and sulfur. The results indicates that different concentrations of LiTFSI in electrolytes present a substantial impact on cycle stability, but the electrochemical charge/discharge reaction processes have not been changed. Among the four electrolytes with different concentrations of lithium salt, the S/KB-1 composite measured in the electrolyte with 5 M LITFSI shows optimal cycle stability. Therefore, the effect of synthesis methods on cycle stability for the S/KB composites was further investigated in the electrolyte.

The cycle performance of S/KB-2 and S/KB-3 composites measured at the current density of 160 mA g^{-1} is shown in Fig. 5a. For the S/KB-2 composite prepared by ball-milling method, a low initial discharge capacity of 518.8 mAh g^{-1} is obtained. However, the discharge capacity of the S/KB-2 composite gradually increases to 684 mAh g^{-1} after 50 cycles. The electrochemical activity of the S/KB-2 composite gradually improved due to the slow penetration and transport of lithium ions through electrolyte/electrode interface, leading to increased utilization with cycling. For the S/KB-3 composite prepared by ball milling-melting method, the initial discharge capacity is 805 mAh g^{-1}, which is higher than that of the S/KB-2 composite. However, the capacity gradually decreases to 489.7 mAh g^{-1} after 50 cycles, due to reduced electrical conductivity of the composite electrode, resulting in poor capacity retention capability. Moreover, the corresponding initial, 10^{th}, and 50^{th} charge-discharge curves of the two samples are shown in Figs. 5b to 5c, respectively. As seen in the figures, the two typical discharge plateaus located at around 2.30 and

2.0 V (versus Li/Li^+) are similar to those of the S/KB-1 composite. However, the low and long potential plateau at around 1.20 V could not be observed in the initial discharge process for both composite electrodes, suggesting the lack of weak interaction between carbon and sulfur in the S/KB-2 and S/KB-3 composites. Apparently, the synthesis methods for sulfur/carbon composites also exert a considerable impact on the cycle stability of Li-S batteries.

To further explore the effect of synthesis methods on the electrochemical reaction process, EIS among the three S/KB composites, which are measured at the current density of 160 mA g^{-1} at the discharged state to 1.0 V, were conducted, and Nyquist plots are presented in Fig. 6. All Nyquist plots are composed of a depressed semicircle at high frequency and an inclined line at low frequency. The semicircle in the high-frequency region is related to the charge transfer, and the inclined line in the low-frequency region refers to Li-ion diffusion in the cathodes. Evidently, S/KB-1 shows considerably smaller high-frequency semicircle as compared with S/KB-2 and S/KB-3, resulting in a lower charge-transfer resistance, faster reaction kinetics, and superior reversibility. This result indicates that the active sulfur in the S/KB-1 composite presents higher dispersion degree and better electrochemical contact than the S/KB-2 and S/KB-3 composites. Thus, the S/KB-1 composite possesses better cycle stability and a higher reversible capacity as cathode material for Li-S batteries.

By comparing the results, the S/KB-1 prepared by melting-vaporizing method presents optimized electrochemical performance when measured in the electrolyte with 5 M LiTFSI in DOL/TEGDME. To better demonstrate the composite electrode, the prolonged charge/discharge cycle curves, corresponding coulombic efficiency, and rate discharge capability are further evaluated. The image in Fig. 7a shows the prolonged cycle performance and coulombic efficiency

of the S/KB-1 composite measured in the electrolyte with 5 M LiTFSI in DOL/TEGDME at a current density of 160 mA g^{-1}. As discussed above, the cell delivers a high initial capacity of 1856.2 mAh g^{-1}, which is higher than the theoretical capacity of active sulfur. In the second cycle, the capacity sharply decreased to 1080.5 mAh g^{-1}, mainly due to the dissolution of polysulfide into the electrolyte and the irreversible capacity loss of carbon to the metallic lithium anode. However, a discharge capacity of 905.3 mAh g^{-1} could still be maintained after 125 cycles, corresponding to 83.8% capacity retention from the second cycle. In particular, coulombic efficiency reaches about 100% for the composite during cycling. As shown in Fig. 7b, the composite presents an initial discharge capacity of 813.6 mAh g^{-1} when measured at a current density of 400 mA g^{-1}, and the discharge capacity can still be maintained at 728.8 mAh g^{-1} after 50 cycles. Furthermore, the high-rate discharge capability and long-term cycle performance of the S/KB-1 composite measured at a high current density of 800 mA g^{-1} is shown in Fig. 7c. As seen, the composite presents a low initial discharge capacity of 346.9 mAh g^{-1}, indicating low utilization of active sulfur for the first cycle. During the first 21 cycles, a considerably decrease in capacity occurs, and the lowest capacity is 202.9 mAh g^{-1}. However, from the 22^{nd} cycle on, the electrochemical activity of the S/KB composite is gradually improved, due to the slow penetration and transport of electrolyte and lithium ions through the pores of the carbon matrix. It should be noted that the use of tetraethylene glycol dimethyl ether (TEGDME) as solvent in the electrolyte is more viscous than the conventional electrolyte with 1,2-dimethoxyethane (DME) as solvent. Therefore, when exerting a high current rate on the cell, the electrochemical activity of the composite electrode would be gradually improved after the efficient penetration and transportation of electrolyte and dissolution of lithium polysulfides. Finally, the discharge capacity increases to

209.4 mAh g^{-1} in the 22nd cycle, and a maximum discharge capacity of 641 mAh g^{-1} is obtained after 394 cycles, leading to the increased utilization of active sulfur. After 500 cycles, the discharge capacity can still remain at 546.3 mAh g^{-1}, showing good high-rate performance and capacity retention capability.

4. Conclusions

Sulfur/carbon composites are prepared by loading sulfur in a commercial carbon black matrix through three different synthesis methods. The obtained S/KB-1 composite, which is prepared by melting (155 °C)-vaporizing (300 °C) method exhibits optimized cycling stability and utilization of active sulfur, as well as rate capability, when measured in the electrolyte with 5 M LiTFSI. On account of the electrochemical results above, the high performance of the S/KB-1 composite is mainly attributed to electrolyte concentration and synthesis method: (1) the high concentration of lithium salt (LiTFSI) can effectively suppress polysulfide dissolution into the electrolyte because of the "common-ion effect", and (2) the melting-vaporizing synthesis method provides active sulfur with more highly dispersed in the S/KB-1 composite and more excellent electrochemical contact with carbon matrix; while ball milling synthesis method only provides active sulfur favourable conductivity in the S/KB-2 composite, and ball milling-melting synthesis method hinders the transportation of electrons and ions in S/KB-3 composite. Finally, both electrolyte concentration and synthesis methods of sulfur/carbon composites exert considerable effect on the capacity and cycle stability of Li-S batteries.

Acknowledgements

The financial supports from NSFC (51403087), the Natural Science Foundation of Jiangsu Province (BK20140563), the Research Funds for Senior Professionals of Jiangsu University (14JDG027), the Priority Academic Program Development of Jiangsu Higher Education Institutions (PAPD) and Jiangsu Province Science and Technology Support Project (BE2014008 and BE2014008-2) in China are gratefully acknowledged.

References

1. X. L. Ji and L. F. Nazar, *J. Mater. Chem.,* 2010, **20**, 9821-9826.
2. X. P. Gao and H. X. Yang, *Energy Environ. Sci*., 2010, **3**, 174-189.
3. P. G. Bruce, S. A. Freunberger, L. J. Hardwick and J. M. Tarascon, *Nat. Mater*., 2012, **11** 19-29.
4. S. S. Zhang, *J. Power Sources*, 2013, **231**, 153-162.
5. A. Manthiram, Y. Z. Fu, S. H. Chung, C. X. Zu and Y. S. Su, *Chem. Rev*., 2014, **114**, 11751-11787.
6. M. A. Pope and I. A. Aksay, *Adv. Energy Mater*., 2015, DOI: 10.1002/aenm.201500124.
7. R. D. Rauh, K. M. Abraham, G. F. Pearson, J. K. Surprenant and S. B. Brummer, *J. Electrochem. Soc*., 1979, **126**, A523-527.
8. J. Shim, K. A. Striebel and E. J. Cairns, *J. Electrochem. Soc*., 2002, **149**, A1321-A1325.
9. X. L. Ji, K. T. Lee and L.F. Nazar, *Nat. Mater*., 2009, **8**, 500-506.
10. B. Zhang, X. Qin, G. R. Li and X. P. Gao, *Energy Environ. Sci*., 2010, **3**, 1531-1537.
11. H. L. Wang, Y. Yang, Y. Y. Liang, J. T. Robinson, Y. G. Li, A. Jackson, Y. Cui and H. J. Dai, *Nano Lett*., 2011, **11**, 2644-2647.
12. S. R. Chen, Y. P. Zhai, G. L. Xu, Y. X. Jiang, D. Y. Zhao, J. T. Li, L. Huang and S. G. Sun, *Electrochim. Acta*, 2011, **56**, 9549-9555.
13. J. Jin, Z. Y. Wen, G. Q. Ma, Y. Lu, Y. M. Cui, M. F. Wu, X. Liang and X. W. Wu, *RSC Adv*., 2013, **3**, 2558-2560.
14. G. C. Li, G. R. Li, S. H. Ye and X. P. Gao, *Adv. Energy Mater*., 2013, **2**, 1238-1245.
15. L. X. Miao, W. K. Wang, A. B. Wang, K. G. Yuan and Y. S. Yang, *J. Mater. Chem. A*., 2013, **1**, 11659-11664.
16. X. F. Wang, X. P. Fang, X. W. Guo, Z. X. Wang, L. Q. Chen, *Electrochim. Acta*, 2013, **97**, 238-243.
17. W. G. Wang, X. Wang, L. Y. Tian, Y. L. Wang and S. H. Ye, *J. Mater. Chem. A*., 2014, **2**, 4316-4323.
18. G. C. Li, J. J. Hu, G. R. Li, S. H. Ye and X. P. Gao, *J. Power Sources*, 2013, **240**, 598-605.
19. W. D. Zhou, Y. C. Yu, H. Chen, F. J. DiSalvo, H. D. Abruna, *J. Am. Chem. Soc*., 2013, **135**, 16736-16743.
20. Y. Yang, G. H. Yu, J. J. Cha, H. Wu, M. Vosgueritchian, Y. Yao, Z. N. Bao and Y. Cui, *ACS Nano*, 2011, **5**, 9187-9193.

21. Y. Z. Zhang, S. Liu, G. C. Li, G. R. Li and X. P. Gao, *J. Mater. Chem. A*., 2014, **2**, 4652-4659.
22. Y. M. Chen, X. Y. Li, K. S. Park, J. H. Hong, J. Song, L. M. Zhou, Y. W. Mai, H. T. Huang and J. B. Goodenough, *J. Mater. Chem. A.*, 2014, **2**, 10126-10130.
23. Z. Liang, G. Zheng, W. Li, Z. W. Seh, H. Yao, K. Yan, D. Kong and Y. Cui, *ACS Nano*, 2014, **8**, 5249-5256.
24. Y. You, W. C. Zeng, Y. X. Yin, J. Zhang, C. P. Yang, Y. W.Zhu and Y. G. Guo, *J. Mater. Chem. A.*, 2015, **3**, 4799-4802.
25. Q. Li, Z. A. Zhang, Z. P. Guo, K. Zhang, Y. Q. Lai and J. Li, *J. Power Sources*, 2015, **274**, 338-344.
26. S. Kim, Y. J. Jung and H. S. Lim, *Electrochim. Acta*, 2004, **50**, 889-892.
27. L. X. Yuan, J. K. Feng, X. P. Ai, Y. L. Cao, S. L. Chen and H. X. Yang, *Electrochem. Commun*., 2006, **8**, 610-614.
28. B. Céline, J. C. Leprêtre, P. Sébastien, F. Alloin, *J. Electrochem. Soc*., 2013, **160**, A430-A436.
29. L. M. Suo, Y. S. Hu, H. Li, M. Armand and L. Q. Chen, *Nat. Commun*., 2013, **4**, 1481.
30. B. A. Trofimov, M. V. Markova, L. V. Morozova, G. F. Prozorova, S. A. Korzhova, M. D. Cho, V. V. Annenkov and A. I. Mikhaleva, *Electrochim. Acta*, 2011, **56**, 2458-2463.
31. M. He, L. X. Yuan, W. X. Zhang, X. L. Hu and Y. H. Huang, *J. Phy. Chem. C*., 2011, **115**, 15703-15709.
32. J. L. Wang, Z. D. Yao, C. W. Monroe, J. Yang and Y. N. Nuli, *Adv. Funct. Mater*., 2013, **23**, 1194-1201.
33. Z. W. Seh, Q. F. Zhang, W. Y. Li, G. Y. Zheng, H. B. Yao and Y. Cui, *Chem. Sci.*, 2013, **4**, 3673-3677.
34. J. Pan, G. Y. Xu, B. Ding, J. P. Han, H. Dou and X. G. Zhang, *RSC Adv.*, 2015, **5**, 13709-13714.
35. Y. M. Lee, N. S. Choi, J. H. Park and J. K. Park, *J. Power Sources*, 2003, **119-121**, 964-972.
36. G. Q. Ma, Z. Y. wen, Q. S. Wang, C. Shen, J. Jin and X. W. Wu, *J. Mater. Chem. A*., 2014, **2**, 19355-19359.
37. Q. Xu, G. C. Hu, H. L. Bi and H. F. Xiang, *Ionics*, 2105, **21**, 981-986.
38. G. C. Wang, Y. Q. Lai, Z. A. Zhang, J. Li and Z. Y. Zhang, *J. Mater. Chem. A*., 2015, **3**, 7139-7144.
39. G. C. Li, H. K. Jing, Z. Su, C. Lai, L. Chen, C. C. Yuan, H. H. Li and L. Liu, *J. Mater. Chem. A*., 2015, **3**, 11014-11020.
40. N. Ding, S. W. Chien, T. S. A. Hor, Z. L. Liu and Y. Zong, *J. Power Sources*, 2014, **269**, 111-116.
41. S. S. Zhang, *Electrochim. Acta*, 2012, **70**, 344-348.

Figure captions

Fig. 1 TG curves of the as-prepared S/KB-1, S/KB-2, and S/KB-3 composites.

Fig. 2 SEM images of KB (a), S/KB-1 composite (b), S/KB-2 composite (c), and S/KB-3 composite (d).

Fig. 3 HAADF-STEM images and corresponding mappings of carbon and sulfur through the whole area (STEM) of the S/KB-1 composite (a), S/KB-2 composite (b), and S/KB-3 composite (c).

Fig. 4 Cycle performance of S/KB-1 composite measured in the electrolytes with 1, 2, 3, and 5 M LiTFSI in DOL/TEGDME at the current density of 160 mA g^{-1} (a), and the corresponding 1^{st}, 10^{th}, and 50^{th} charge/discharge potential profiles (b to e).

Fig. 5 Cycle performance of S/KB-2 and S/KB-3 composites measured in the electrolyte with 5 M LiTFSI in DOL/TEGDME at a current density of 160 mA g^{-1} (a), and the corresponding 1^{st}, 50^{th} and 10^{th} charge/discharge potential profiles (b to c).

Fig. 6 EIS spectra of S/KB composites prepared by different synthesis methods after being discharged to 1.0 V at a current density of 160 mA g^{-1}.

Fig. 7 Prolonged cycle performance and corresponding coulombic efficiency of the S/KB-1 composite measured in the electrolyte with 5 M LiTFSI in DOL/TEGDME at a current density of

160 mA g^{-1} (a), rate capability of S/KB-1 composite measured at the current density of 400 (b) and 800 mA g^{-1} (c).

Tab. 1 Specific surface areas and pore volumes of KB and as-prepared S/KB composites in each synthesis method. (S_{BET} is the specific surface area, and Vt is the total pore volume.)

Figure

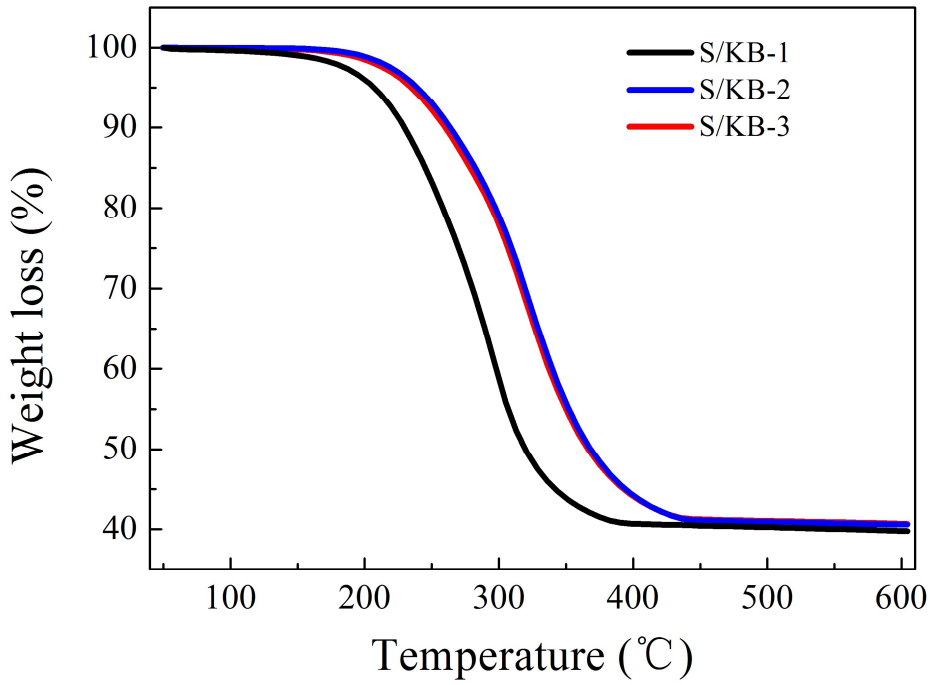

Fig. 1

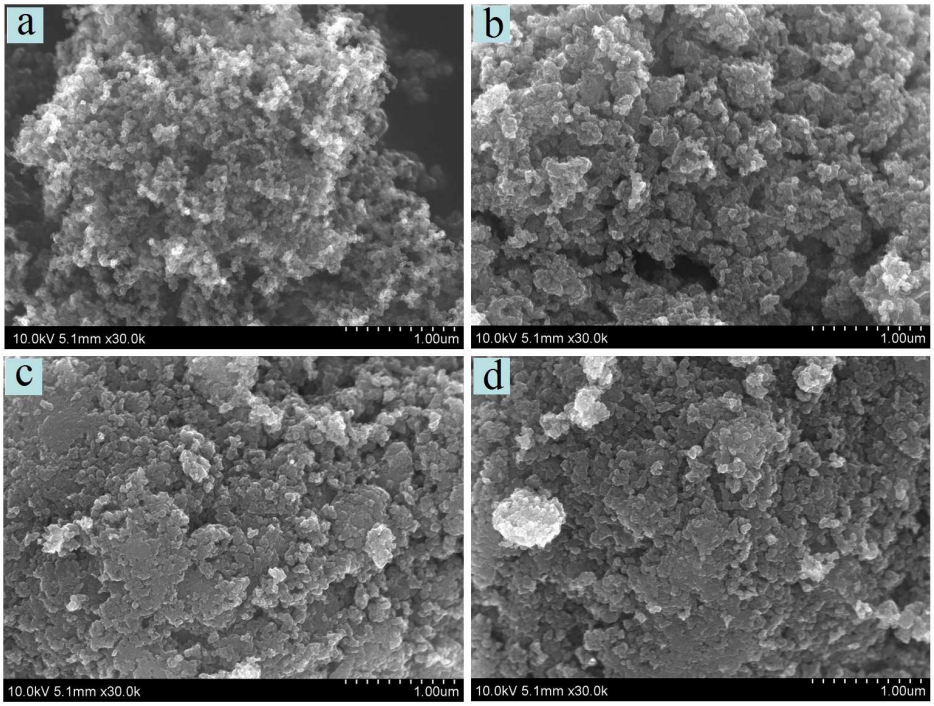

Fig. 2

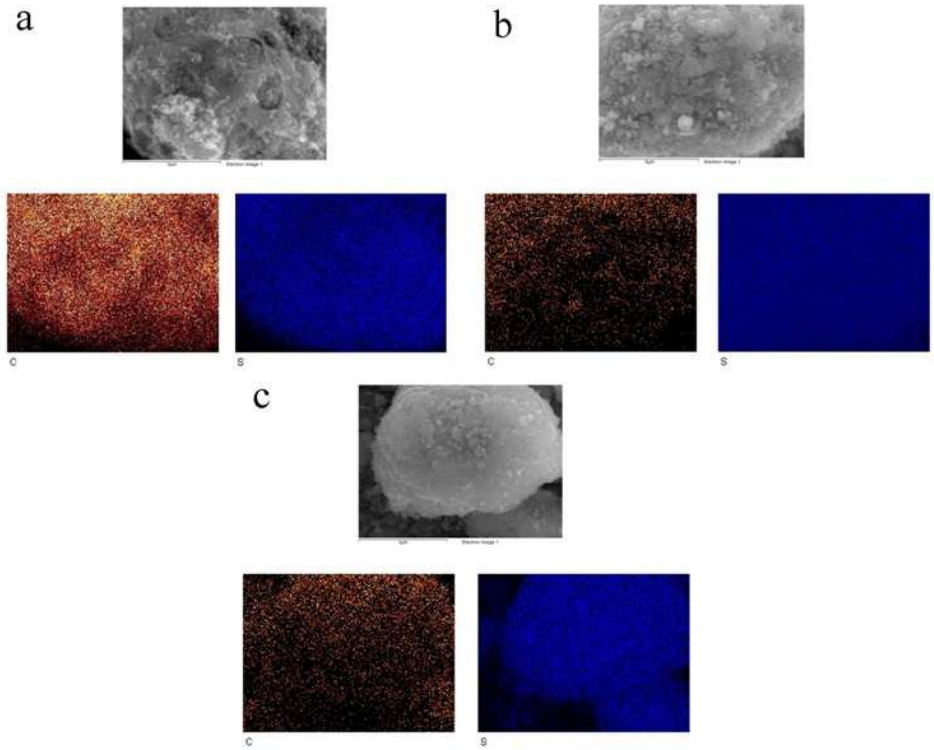

Fig. 3

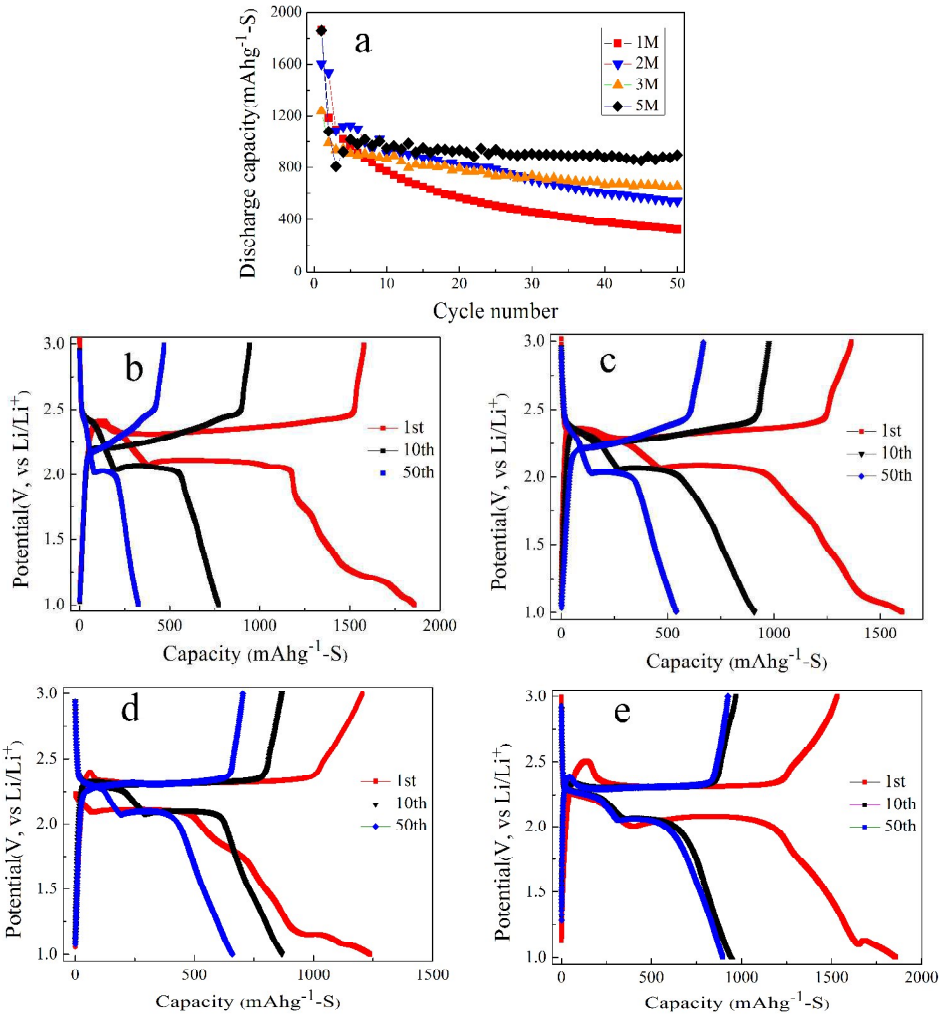

Fig. 4

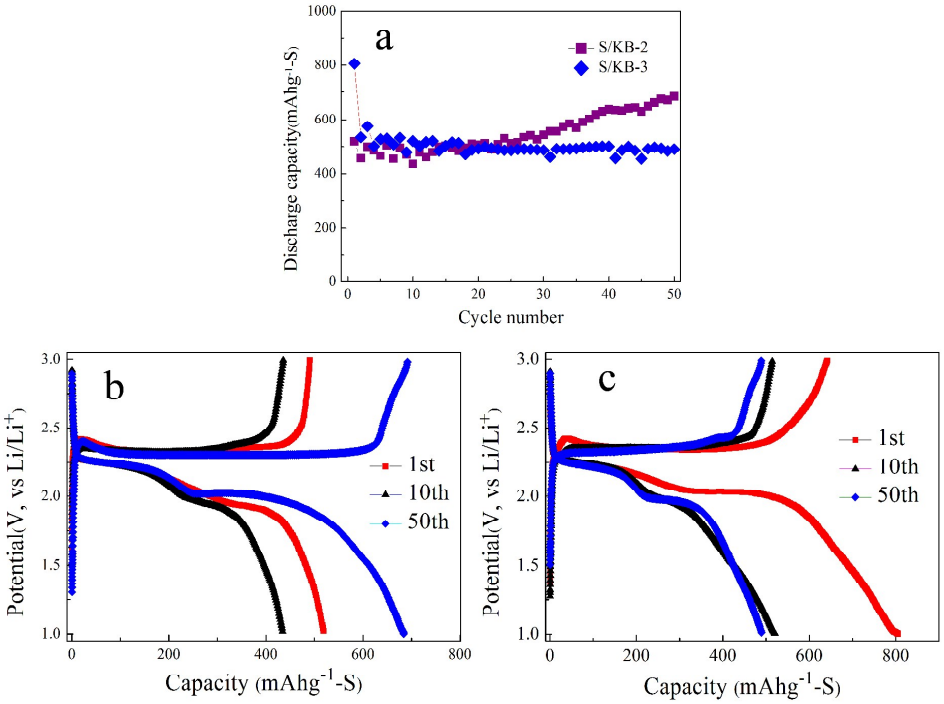

Fig. 5

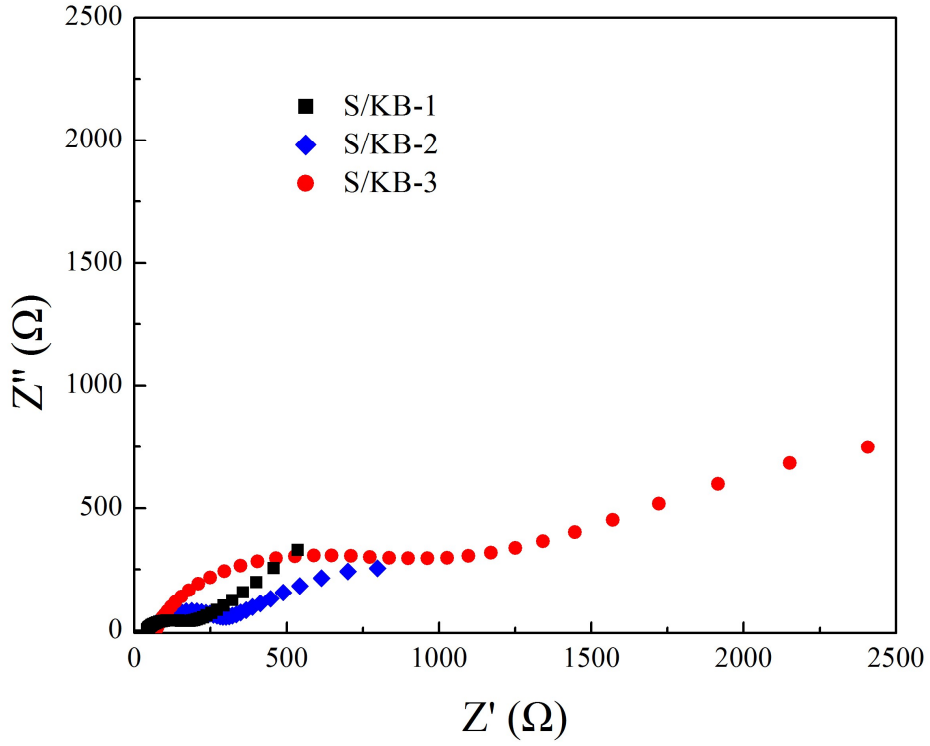

Fig. 6

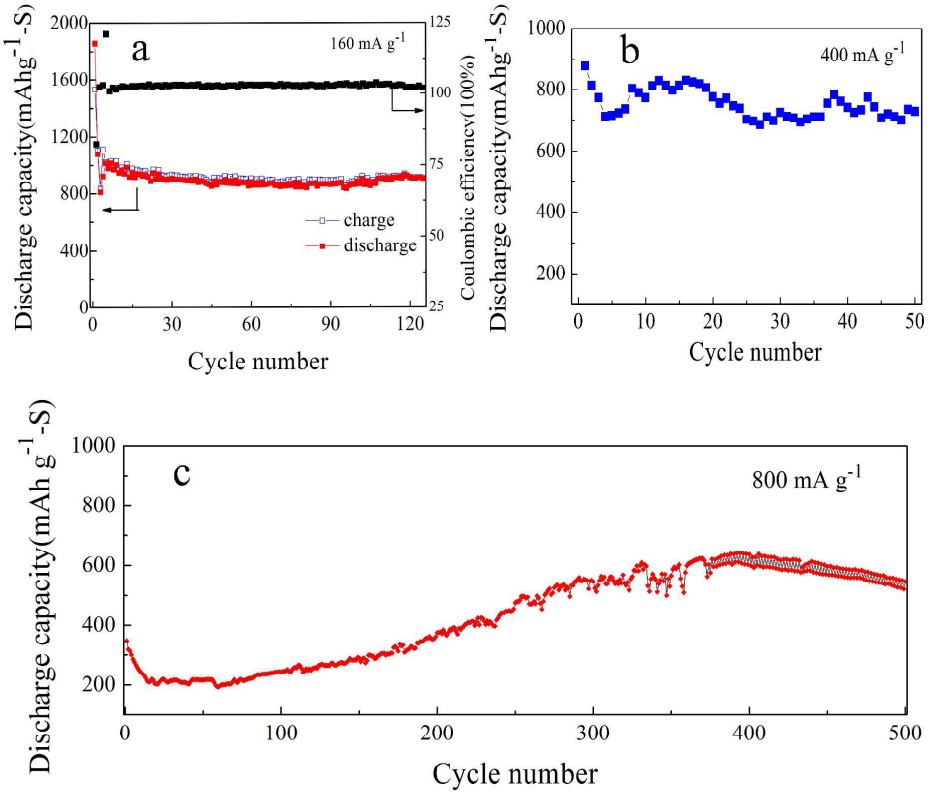

Fig. 7

Sample	S_{BET} (m^2 g^{-1})	V_t (cm^3 g^{-1})
KB	1007.21	2.03
S/KB-1, melting (155 °C)-vaporizing (300 °C)	196.84	0.259
S/KB-2, ball-milling	205.69	0.315
S/KB-3, ball-milling-melting (155 °C)	221.39	0.348

Tab. 1

Table of content

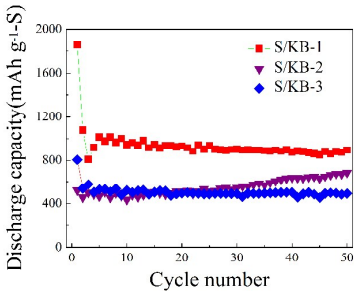

S/KB-1 composite prepared by melting-vaporizing method exhibits the optimized electrochemical performance in the electrolyte with 5 M LiTFSI in DOL/TEGDME.